Preprints of the 19th World Congress
The International Federation of Automatic Control
Cape Town, South Africa. August 24-29, 2014

Nonlinear Estimation of a Parsimonious Wiener Model for the Neuromuscular Blockade in Closed-loop Anesthesia ⋆

Olov Rosén, * **Margarida M. Silva,** *,** **and Alexander Medvedev** *

* *Department of Information Technology, Uppsala University, SE-751 05 Uppsala, Sweden (e-mail: {olov.rosen,margarida.silva,alexander.medvedev}@it.uu.se).*
** *Departamento de Matemática, Faculdade de Ciências da Universidade do Porto, Rua do Campo Alegre, 4169-007 Porto, Portugal, and Center for Research and Development in Mathematics and Applications (CIDMA), Campus Universitário de Santiago, 3810-193 Aveiro, Portugal*

Abstract: The recursive identification of a parsimonious nonlinear Wiener model for the neuromuscular blockade in closed-loop anesthesia is considered. The performance of two popular nonlinear estimation techniques, namely the extended Kalman filter (EKF) and the particle filter (PF), is evaluated on synthetic and clinical data. The parameter estimates obtained with the PF, that does not rely on model linearization, exhibit less bias and shorter settling time than the ones produced by the EKF. This behavior persists when the parameter tracking capabilities of both estimation algorithms are assessed for the model in hand. Taking advantage of the model parameters that were recursively estimated from clinical data, it is demonstrated that the main source of intra-patient variability lies in the nonlinear pharmacodynamic part of the model. The distance to a bifurcation phenomenon leading to nonlinear oscillations of the Wiener model under PID feedback is also evaluated.

Keywords: Biomedical control, Dynamical systems, Estimation algorithms, Parameter estimation, Nonlinear oscillations.

1. INTRODUCTION

The recursive estimation of a parsimonious nonlinear Wiener model for the neuromuscular blockade (NMB) in closed-loop anesthesia is addressed in this paper.

Nonlinear dynamical models provide a broad framework for biological and physiological systems and are well suited for the problem of drug delivery control, Haddad et al. (2006). While pharmacokinetic/pharmacodynamic (PK/PD) models offer a detailed insight into the underlying physiological processes, they usually raise identifiability concerns whenever the aim of parameter estimation from measured input-output data of the system is model individualization, Silva et al. (2014). Therefore, minimal parsimonious models for the effect of drugs in anesthesia were proposed in Silva et al. (2012) and Silva et al. (2010). Other reduced models followed, namely Hahn et al. (2012) and Hodrea et al. (2013), further supporting the idea that simple model structures can capture the most significant dynamics of the system, i.e. the human body, in response to drug administration, allowing at the same time model individualization.

Owing to the nonlinear nature of the system, it is expected that estimation algorithms making direct use of the nonlinear model perform better than estimation methods that rely on linearization. The first contribution of this paper is hence the estimation of the parsimonious Wiener model for the NMB proposed in Silva et al. (2012) with a particle filter (PF) compared with that by an extended Kalman filter (EKF). While the PF exploits the nonlinear model structure, the EKF calculates the feedback gain from a linearization of the nonlinear model dynamics around the state estimates at each time instant.

The inter-patient variability in response to administration of drugs in anesthesia greatly complicates the automatic drug delivery and necessitates individualized control of it. The phenomenon has been extensively assessed for the two main components of anesthesia: the NMB, in e.g. Caiado et al. (2012) and Silva et al. (2013); and the depth of anesthesia (DoA), in e.g. Niño et al. (2009), Dumont et al. (2009), and van Heusden et al. (2013). The performance of an individualized feedback controller is, in fact, directly influenced by the intra-patient variability, i.e. the uncertainty incurred by the changes in the PK/PD characteristics of the patient throughout a general anesthesia

⋆ The authors were in part financed by the European Research Council, Advanced Grant 247035 (SysTEAM). M. M. Silva was also in part financed by Portuguese funds through CIDMA and Fundação para a Ciência e a Tecnologia (FCT), within project PEst-C/MAT/UI4106/2011 with COMPETE number FCOMP-01-0124-FEDER-022690.

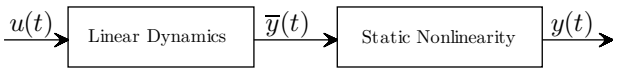

Fig. 1. Block diagram of a Wiener model.

episode, due to e.g. variations in cardiac output, and/or co-administered drugs, Absalom et al. (2011).

Considering the tracking capabilities of the PF and the EKF, the intra-patient PK/PD variability in terms of model parameter estimates variation is also assessed here, being this the second contribution of the paper.

Recent research has shown that complex nonlinear dynamics may arise in the closed-loop system of a Wiener model for the NMB controlled by a PID feedback. According to Zhusubaliyev et al. (2013), there exists a region in the parameter space where the system possesses a single stable equilibrium and, when varying the parameters, this equilibrium undergoes a bifurcation that leads to the emergence of self-sustained nonlinear oscillations. Notably, oscillating PID loops in closed-loop anesthesia have been observed in clinical experiments, e.g. Absalom and Kenny (2003). The third contribution of this paper is hence a quantification of the distance to bifurcation for the identified models. This quantification provides insight into how close to a nonlinear oscillation the closed-loop system is and may be used as a flag in a safety net for PID controlled anesthesia.

The remainder of this paper is organized as follows. Section 2 describes the parsimonious nonlinear Wiener model that is used to parametrize the effect of the muscle relaxant atracurium in the NMB. Section 3 introduces briefly the EKF and the PF, while Section 4 summarizes the data sets and the performance metrics that were used to assess parameters convergence as well as filtering and tracking capabilities of both considered parameter estimation techniques. Section 5 presents the estimation results and, finally, the conclusions are drawn in Section 6.

2. PARSIMONIOUS WIENER MODEL

A block diagram of a Wiener model is shown in Fig. 1. In the parsimonious Wiener model for the NMB, Silva et al. (2012), that is used in this paper, the model input $u(t)$ [μg kg^{-1}min^{-1}] is the administered atracurium rate, and the model output $y(t)$ [%] is the NMB level. It should be noted that the intermediate signal $\overline{y}(t)$ is not accessible for measurement.

The transfer function of the linear model dynamics is

$$\overline{Y}(s) = \frac{k_1\, k_2\, k_3\, \alpha^3}{(s + k_1\,\alpha)(s + k_2\,\alpha)(s + k_3\,\alpha)}\, U(s), \qquad (1)$$

where $\overline{Y}(s)$ is the Laplace transform of the continuous-time output $\overline{y}(t)$ of the linear dynamic part of the model and $U(s)$ is the Laplace transform of the input signal $u(t)$. The latter is nonnegative and bounded, i.e. $0 \leqslant u(t) \leqslant u_{\max}$.

The constants k_i, $\{i = 1, 2, 3\}$ are positive, and α [min^{-1}] > 0 is the patient-dependent parameter in the linear block. In the analysis that follows, the values chosen in Silva (2011), $k_1 = 1$, $k_2 = 4$ and $k_3 = 10$ are assumed.

The effect of the drug is quantified by the measured NMB $y(t)$ [%] and modeled by the Hill function as

$$y(t) = \frac{100\, C_{50}^{\gamma}}{C_{50}^{\gamma} + \overline{y}(t)^{\gamma}}\,, \qquad (2)$$

where γ (adimensional) is the parameter to be identified in the nonlinear block; $y(t)$ is the output of the nonlinearity, $\overline{y}(t)$ is the continuous-time output of the linear dynamic part of the model (1), and C_{50} [μg kg^{-1}min^{-1}] is a normalizing constant that is equal to 3.2435 in simulations.

In order to implement the model structure of (1), (2) in the estimation algorithms, the continuous-time representation expressed by (1) was sampled using a zero-order hold method, Åström and Wittenmark (1984). The discrete-time model becomes

$$\begin{aligned} \overline{x}_{k+1} &= \Phi(\alpha)\overline{x}_k + \Gamma(\alpha)u_k, \qquad (3)\\ \overline{y}_k &= C(\alpha)\overline{x}_k, \end{aligned}$$

where

$$\Phi(\alpha) = e^{A(\alpha)h}, \qquad (4)$$

$$\Gamma(\alpha) = \int_0^h e^{A(\alpha)s}\, ds\, B(\alpha), \qquad (5)$$

and $u_k \in \mathbb{R}$ is the input (piecewise constant atracurium dose), $\overline{x}_k \in \mathbb{R}^{3\times 1}$ is the discrete-time state-vector in a minimal state-space representation, $\overline{y}_k \in \mathbb{R}$ is the discrete-time output of the linear block, $\Phi(\alpha) \in \mathbb{R}^{3\times 3}$ and $\Gamma(\alpha) \in \mathbb{R}^{3\times 1}$ are the sampled system matrices, and $A(\alpha) \in \mathbb{R}^{3\times 3}$ and $B(\alpha) \in \mathbb{R}^{3\times 1}$ are the continuous-time state-space system matrices. The subscript $(\cdot)_k$ denotes the kth sample. Due to the fact that, in the surgery environment, NMB data are monitored and acquired every 20 seconds to ensure that all the nerve fibers are recruited every time an electrical stimulation is performed, the zero-order hold method is applied using $h = 1/3$ min^{-1}.

The sampling does not affect the nonlinear block, hence (2) can be used as it is. The model output is then given by:

$$y_k = \frac{100\, C_{50}^{\gamma}}{C_{50}^{\gamma} + \overline{y}_k^{\gamma}}\,. \qquad (6)$$

To enable the estimation of the model parameters, a coupled identification model is defined. The model merges the sampled model of (3) and (6) with a random walk model for the parameter estimates, Söderström and Stoica (1989). The resulting augmented state vector (denoted by x) becomes

$$x_k = \begin{bmatrix} \overline{x}_k^T & \alpha_k & \gamma_k \end{bmatrix}^T. \qquad (7)$$

Using (7), the extended state-space model is the following:

$$\begin{aligned} x_{k+1} &= \begin{bmatrix} \Phi(\alpha_k) & 0_{3\times 2} \\ 0_{2\times 3} & I \end{bmatrix} \begin{bmatrix} \overline{x}_k \\ \alpha_k \\ \gamma_k \end{bmatrix} + \begin{bmatrix} \Gamma(\alpha_k) \\ 0_{2\times 1} \end{bmatrix} u_k + v_k \\ &\equiv f(x_k, u_k) + v_k, \qquad (8)\\ y_k &= \frac{100\, C_{50}^{\gamma_k}}{C_{50}^{\gamma_k} + \left(C(\alpha_k)x_k\right)^{\gamma_k}} + e_k \\ &\equiv h(x_k) + e_k\,, \qquad (9) \end{aligned}$$

where $v_k \in \mathbb{R}^5$ and $e_k \in \mathbb{R}$ are white zero-mean Gaussian noise processes, with the probability density functions denoted by $p_v(v)$ and $p_e(e)$, respectively.

3. ESTIMATION ALGORITHMS

The EKF and the PF are two widely used algorithms for nonlinear state estimation problems.

The EKF builds on the idea of adapting Kalman filtering to nonlinear models. At each time step, the filter gain is computed by linearizing the nonlinear model around the previous state estimates. Unlike the Kalman filter, the EKF is not an optimal filter and assumes that both the process and sensor noises are Gaussian.

The PF uses Monte Carlo simulation to obtain a sample from the posterior distribution, from which the state estimate can be extracted. It provides a general framework for estimation in nonlinear non-Gaussian systems. The PF does not make any approximations to the underlying model, but yields an approximation to the true solution of the filtering problem. The approximation can be made arbitrarily accurate by increasing the number of particles, but comes with the cost of an increasing computational burden, that is the main drawback of the method. However, the PF can be parallelized on e.g. multicore computers with linear speedup in the number of cores Rosen et al. (2010), Rosen and Medvedev (2013).

3.1 Extended Kalman filter (EKF)

The EKF assumes that v_k and e_k in (8) and (9) are mutually independent Gaussian white noise sequences with zero mean and the covariances Q and R, respectively. The algorithm may hence be summarized as follows (cf. e.g. Söderström (2002)):

$$\begin{aligned} H_k &= \left.\frac{\partial h(x)}{\partial x}\right|_{x=\hat{x}_{k|k-1}} \\ K_k &= P_{k|k-1}H_k^T[H_kP_{k|k-1}H_k^T + R]^{-1} \\ \hat{x}_{k|k} &= \hat{x}_{k|k-1} + K_k[y_k - h(\hat{x}_{k|k-1})] \\ P_{k|k} &= P_{k|k-1} - K_kH_kP_{k|k-1} \\ \hat{x}_{k+1|k} &= f(\hat{x}_{k|k}, u_k) \\ F_k &= \left.\frac{\partial f(x,u_k)}{\partial x}\right|_{x=\hat{x}_{k|k}} \\ P_{k+1|k} &= F_kP_{k|k}F_k^T + Q. \end{aligned} \tag{10}$$

In this case, the linearization of $f(x_k, u_k)$ and $h(x_k)$ from (8) and (9) was performed analytically. The formulas for F_k and H_k are omitted here for brevity.

3.2 Particle filter (PF)

For the present application, the commonly used sampling importance resampling (SIR) PF was implemented. Let $x^{(i)}$ denote a particle, $w^{(i)}$ the corresponding weight, and N the number of particles. Then, following Ristic et al. (2004), the estimation algorithm is

$$\begin{aligned} \tilde{x}_{k+1}^{(i)} &= f(x_k^{(i)}, u_k) + v_k^{(i)} \\ \tilde{w}_{k+1}^{(i)} &= w_k^{(i)}p_e(y_k - h(\tilde{x}_k^{(i)}, u_k)) \\ w_{k+1}^{(i)} &= \tilde{w}_{k+1}^{(i)}/\sum_{j=1}^{N}\tilde{w}_{k+1}^{(j)} \\ \hat{x}_{k+1} &= \sum_{j=1}^{N} w_{k+1}^{(j)}x_{k+1}^{(j)}. \end{aligned} \tag{11}$$

In the three first equations above, i ranges over $1, 2, .., N$, and $v_k^{(i)}$ is a draw from $p_v(v)$. The particles are then resampled, via a bootstrapping procedure, by drawing N new particles $\{x_{k+1}^{(i)}\}_i^N$, with replacement such that $\Pr(x_{k+1}^{(i)} = \tilde{x}_{k+1}^{(i)}) = w_{k+1}^{(i)}$, where $\Pr(\cdot)$ is the probability operator, and the weights are set to $w_{k+1}^{(i)} = 1/N$.

3.3 Tuning

The EKF and the PF with 4×10^4 particles were tuned individually over a synthetic database (see Section 5) aiming at the best performance in terms of convergence speed and bias with reasonable output filtering. For the sake of evaluation consistency, this tuning was used for all simulations in this paper. Notably, the initial covariance matrix of the EKF was not increased further, which would result in a reduced settling time of the estimates. This is because, with a more aggressive tuning, the estimates of the nonlinear parameter γ diverged, in some cases, during the initial transient.

The tuned covariances matrices for the EKF are as follows:

$$\begin{aligned} P_{1|0} &= \mathrm{diag}\left(10^{-4}\ 10^{-4}\ 10^{-4}\ 10^{-4}\ 10^{0}\right), \\ Q &= \mathrm{diag}\left(10^{0}\ 10^{0}\ 10^{0}\ 10^{-6}\ 10^{-1}\right), \\ R &= 10^2, \end{aligned} \tag{12}$$

where $\mathrm{diag}(\cdot)$ denotes a diagonal matrix with the specified elements of the main diagonal.

The tuned covariance matrices for the PF are as follows:

$$\begin{aligned} P_{1|0} &= \mathrm{diag}\left(10^{-4}\ 10^{-4}\ 10^{-4}\ 10^{-2}\ 10^{0}\right), \\ Q &= \mathrm{diag}\left(10^{-3}\ 10^{-3}\ 10^{-3}\ 10^{-8}\ 10^{-3}\right), \\ R &= 0.7. \end{aligned} \tag{13}$$

The initial estimates of the parameters were calculated as the mean over the synthetic database (see Section 4.1), i.e. 0.0378 for α and 2.8338 for γ.

4. DATA SETS AND PERFORMANCE EVALUATION METRICS

The two data sets and the metrics used for the performance evaluation of the EKF and the PF are described below.

4.1 Synthetic Data

Synthetic data were obtained by simulating the system given by (1) and (2) with the parameters database of 48 cases in Rocha et al. (2013), to assess the convergence properties in terms of bias and settling time, as well as the tracking properties of both algorithms. The parameter sets

of $\left(\alpha^{(i)}, \gamma^{(i)}\right)$, $\{i = 1, \ldots, 48\}$ were initially obtained by a prediction error method, as explained in Silva (2011), using input-output real data collected in PID controlled closed-loop NMB and further optimized in Rocha et al. (2013). The input (i.e. drug dose) used to generate the 48 synthetic data sets was the same as the one administered in the 48 real cases to guarantee that the excitatory properties of the real input signals are preserved.

Convergence properties: In order to assess the convergence properties in terms of bias and settling time of both the EKF and the PF, the model parameters α and γ were kept constant during the whole simulation.

The settling time for an estimate $\hat{\theta}_k$ of a scalar parameter θ is here defined as the time $t_s = k_s h$, where k_s is the smallest value for which

$$\max_{k \geq k_s} \hat{\theta}_k - \min_{k \geq k_s} \hat{\theta}_k \leq K \tag{14}$$

is satisfied, i.e. the smallest k_s for which the signal will be confined to a corridor of width K, for k larger than or equal to k_s. If the signal settles, the bias in the estimate is defined as

$$b_\theta = \theta - \frac{1}{N^* - k_s} \sum_{k=k_s}^{N^*} \hat{\theta}_k \,, \tag{15}$$

where N^* is the number of samples from k_s to the end of the case being evaluated.

Tracking properties: In order to assess the tracking properties of both algorithms, the true value of γ for the model simulation is made to evolve following a sigmoidal decay of 20% after minute 50, i.e. time step $k_0 = 150$, according to

$$\gamma_k = \begin{cases} \rho \,, & k \leq k_0, \\ \rho \left(1 - 0.2 \dfrac{1}{1 + (\frac{k_0}{k - k_0})^3} \right) \,, & k > k_0, \end{cases} \tag{16}$$

where $\rho = \gamma^{(i)}$ for case i. This is to simulate slow drifts in the patients' dynamics that might occur during a general anesthesia episode. The parameter in the nonlinear block is chosen for this test over the parameter in the linear one (i.e. α) to highlight the nonlinear estimation performance of the evaluated algorithms.

Distance to bifurcation: Following Zhusubaliyev et al. (2013), the condition for the birth of sustained nonlinear oscillations of the PID closed-loop system is given by a surface that is nonlinear in the model parameter α and the controller gains R and L, as defined in the Ziegler-Nichols tuning procedure. The choice of this tuning procedure follows the work of Mendonça and Lago (1998). The 48 models in the synthetic database were used to obtain the $\left(R^{(i)}, L^{(i)}\right)$, $\{i = 1, \ldots, 48\}$ via Ziegler-Nichols. Considering a nominal model i, the nominal controller gains $\left(R^{(i)}, L^{(i)}\right)$ define a point in the (R, L) 2-D space. The parameter estimates $\hat{\alpha}_k$ from the PF estimation give rise to different bifurcation conditions that, in the case of a fixed $\hat{\alpha}_k$ at each sampling time k, degenerate to lines in the (R, L) space. To assess how close the nominal model defined by (R_j, L_j) is to the bifurcation condition at each time instant, the minimum of the Euclidean distance between this point and the bifurcation line was numerically calculated by a grid search.

4.2 Real data

The database of real cases includes 48 datasets collected from patients subject to PID-controlled administration of the muscle relaxant atracurium under general anesthesia. The demographics of the patients is 25 Male, 22 Female, 69±11 kg ([50,94]), 59±15 years ([18,92]). Between brackets are the [min,max] values of the presented data. It should be noted that the demographic data for one patient in the 48 cases database were not registered by the time the cases were collected. A detailed explanation on how this data set was obtained can be found in Rocha et al. (2013).

Real data were used to validate the conclusions drawn from the synthetic data experiments. The output errors obtained in the EKF and PF filtering were compared for different phases of anesthesia reflected in the data set. Similarly to Mendonça and Lago (1998), four phases were defined. Phase 1, $0 < t \leq 10$ min, covers the induction, where the system is driven by the bolus of 500μg/kg that is manually administrated at time zero. Phase 2, $10 < t \leq 30$ min, comprises an intermediate phase where only a P-controller was used. Phase 3, $30 < t \leq 75$ min, starts when the recovery from the intial bolus is supposed to take place, and ends when the reference reaches its final value of 10%. Phase 4, $75 < t \leq t_{\text{end}}$, corresponds to steady-state. In the real cases, the system was PID-controlled during phase 3 and 4, i.e. for $t \geq 30$ min.

5. RESULTS

This section presents the results of the EKF and the PF estimation of the nonlinear Wiener model for the NMB described in Section 2.

5.1 Synthetic data

Figure 2 shows the parameter estimates of case number 34 in the synthetic database. The estimates obtained by the PF, in solid blue line, converge faster than the estimates obtained by the EKF, in dashed green line, and exhibit less bias, as defined in (15). This behavior persists in most of the cases in the database. Figure 3 illustrates this by showing the true α and γ vs. bias (15) in the estimates for the PF and EKF for the 48 cases in the database. It is hence evident that the PF, in general, yields estimates with less bias than the EKF, this being especially prominent for large values of α and γ. The presence of a higher bias in the estimates of the EKF for higher values of the nominal parameters may be explained by the fact that the gain of the EKF is calculated from a linearized version of the nonlinear Wiener model while the PF performs no linearization at all.

Figure 4 depicts the estimates of γ for a case where the true value, plotted in dotted red, is made to change obeying a sigmoidal function after minute 50, according to (16). The estimates obtained by the EKF are plotted in dashed green, while the estimates obtained by the PF are

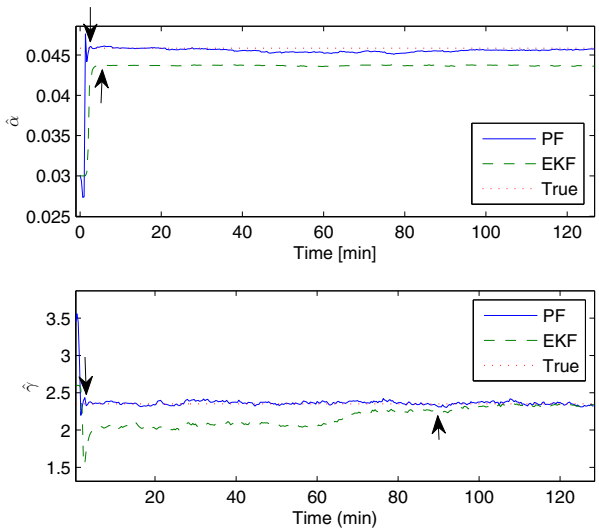

Fig. 2. Estimated α (upper plot) and γ (bottom plot) for the EKF (in dashed green line) and the PF (in solid blue line) for case number 34 in the synthetic database. The points where the estimates settle, according to (14), are pointed out by the arrows. The true parameter values are plotted in dotted red line.

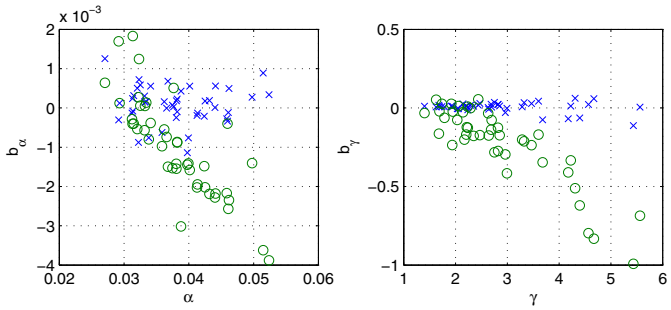

Fig. 3. The true α and γ vs. estimation bias b_α and b_γ, respectively, for the 48 cases in the synthetic database. The results for the EKF are plotted in green circles and the results for the PF are plotted in blue crosses.

plotted in solid blue. This is a case representative of the behavior of the estimates in all the 48 cases in the synthetic database. As in the case of time-invariant parameters, the EKF presents a higher bias at tracking the change than the PF. This higher bias might be explained by the fact that the PF possesses faster error dynamics than the EKF. Since the simulations are limited by the length of the input signals that were administered in the real general anesthesia scenarios, as mentioned in Section 4.1, the simulations could not be run for longer time in order to assess whether the bias in the EKF estimate would be reduced with time.

5.2 Real data

Keeping the tuning unchanged, the EKF and the PF were applied to the 48 cases of real input-output data. Figure 5 shows the estimates of α and γ over time for case number 39 in the real database. Due to the fact that the input-output data used to perform the estimation came from a real case, the true parameter values are not

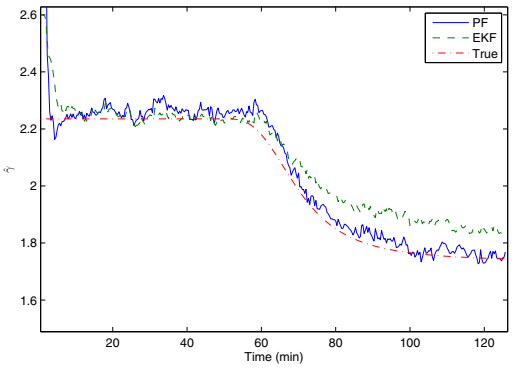

Fig. 4. Estimated γ for the EKF in dashed green line, and for the PF in solid blue line. At minute 50 the true γ, in dotted red line, drifts from its initial value according to (16).

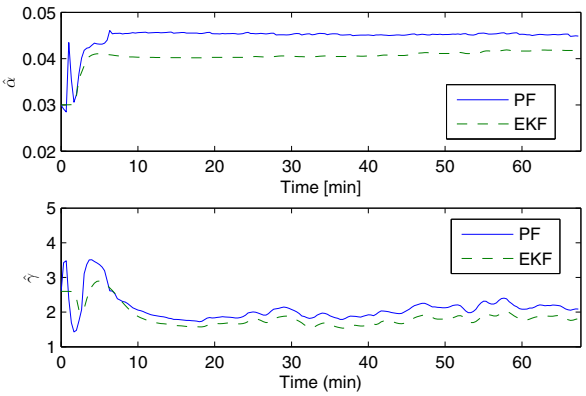

Fig. 5. Estimated model parameters for the EKF, in dashed green, and the PF, in solid blue, over time for a case number 39 in the real database.

plotted in Fig. 5. The higher variance of the estimates of γ when compared to that of the estimates of α supports the choice of only assessing the tracking performance of both estimation techniques with respect to changes in γ, as argued in Section 4.1.2. The intra-patient variability is hence mostly due to changes in the nonlinear parameter describing the PD part of the model.

Figure 6 shows the mean of the absolute value of the output error with the 1σ confidence interval over all 48 cases. Numerical values of the output errors are also given in Table 1 for the four different phases described in Section 4.2. The general result is that the PF exhibits a much lower output error during the induction phase, i.e. for $0 < t < 10$ min, when compared with the output error that is obtained with the EKF estimates. For $10 \leq t < 30$ min, the EKF provides slightly better output errors, possibly due to less prominent nonlinear dynamics exhibited in this interval. For $t \geq 30$ min, the performance is similar for the EKF and the PF. The better performance of the PF during the highly nonlinear induction phase is likely due to that the PF is designed to handle nonlinear systems without recourse to linearization.

Given the fact that the PF outperforms the EKF in terms of bias, tracking and convergence time, the intra-patient

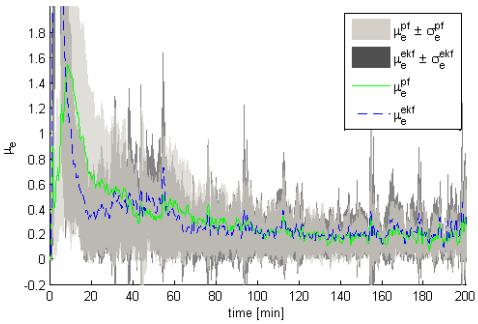

Fig. 6. The mean μ_e^{ekf} and μ_e^{pf} of the absolute value of output error over the 48 cases for the EKF and PF, respectively. The 1σ confidence intervals are given by the transparent areas.

Table 1. Output error of estimation for the EKF and the PF during the four phases defined in Section 4.2.

	EKF			PF		
Phase	mean	stdv	[min,max]	mean	stdv	[min,max]
1	4.16	0.62	[2.58,5.42]	0.95	0.47	[0.24,2.34]
2	0.49	0.17	[0.16,0.85]	0.58	0.39	[0.14,1.97]
3	0.31	0.16	[0.08,0.98]	0.30	0.16	[0.13,0.77]
4	0.25	0.16	[0.04,0.97]	0.25	0.13	[0.07 0.76]

Table 2. Mean, standard deviation and min-max values for the variability in % of $\hat{\alpha}$, $\hat{\gamma}$, in the real database, during the maintenance phase ($t > 30$ min).

	mean	stdv	[min,max]
var($\hat{\alpha}$)	0.007	0.0032	[0.0026,0.0145]
var($\hat{\gamma}$)	0.086	0.037	[0.035,0.187]

variability was only assessed using the estimates provided by the PF.

Table 2 shows the relative mean, standard deviation and min-max values of the parameter estimates in % for $t > 30$ min, i.e. during the maintenance phase. The mean value of the variance of the estimates for the nonlinear parameter γ is higher than for the linear parameter α which observation supports the claim that the linear dynamics (PK) are the most conserved among patients, while the nonlinear dynamics (PD) are the most different between patients. These values should be taken into account when designing robust controllers for the administration of drugs for the NMB.

In order to get some insight on the need of estimating the model parameters throughout the whole surgery and, consequently, the development of adaptive control strategies, the system was simulated with the estimates of α and γ obtained after induction (at time t=10 min), and the estimates obtained from last time step of the estimation (at $t = t_{\text{end}}$). The mean and standard deviation over the 48 cases of the output errors are shown in Tab. 3. This result shows that, from minute 10 to the end of the surgery, the changes in the model parameters affect the goodness of fit of the simulated model to the real data. It is therefore plausible that adaptive controllers would perform better during maintenance phase than non-adaptive ones, especially under longer surgical interventions.

Table 3. Mean, standard deviation of simulation output error, with the parameters $\hat{\theta}_t = \{\hat{\alpha}_t, \hat{\gamma}_t\}$ obtained at $t = 10$ min, and $t = t_{\text{end}}$

	mean	stdv
$\hat{\theta}_{10}$	2.32	0.13
$\hat{\theta}_{t_{end}}$	4.13	0.22

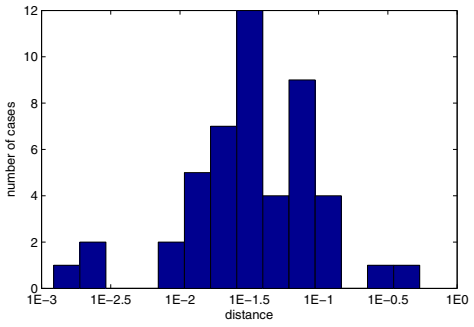

Fig. 7. Histogram of the distance to bifurcation, at time $t = 40$ min, over the 48 cases in the synthetic database, assuming PID control. Note the log-scale on the x-axis.

Given the time-varying nature of the patient dynamics, in a PID control setup, and for safety reasons, it is important to judge whether the system is driven into a parameter region where a bifurcation might lead to nonlinear oscillations. The distance to bifurcation is calculated according to Zhusubaliyev et al. (2013) for the 48 cases at $t = 40$ min and presented in a histogram in Fig. 7. The histogram is representative for all time instants $t > 10$ min, as the distance depends only on $\hat{\alpha}$ which typically settles before $t = 10$ min. It can be seen that most of the cases are further than 10^{-2} from the critical surface. Three cases are nevertheless closer to the surface, which may be of concern in real practice.

It should be noted that the better performance of the PF comes with a higher computational cost than that of the EKF. For this application the EKF and PF require about 10^3 and 10^6 floating point operations per iteration respectively. For an unoptimized Matlab implementations the EKF and PF was clocked to run one iteration of the filtering in 0.39 ms and 1.34 s. For the implementations in hand, the execution time for the PF is hence four orders of magnitude greater than the EKF. In this application, and since the sampling period is 20 s, this difference in execution time is not an issue.

6. CONCLUSIONS

The recursive estimation of a parsimonious nonlinear Wiener model for the NMB in closed-loop anaesthesia is studied on synthetic and real datasets. It is shown that the PF outperforms the EKF at estimating the model parameters when it comes to convergence rate, bias, and tracking capability. Using the parameter estimates obtained by the PF, the intra-patient variability of the model is quantified. The results strongly indicate that the variability in the nonlinear pharmacodynamic part of the model is higher than that of the linear part. It is also demonstrated that the accurate parameter estimates provided by the PF can

under the PID-feedback be utilized for calculating the distance to a nonlinear oscillation and therefore characterize robustness of the closed-loop system in real time.

REFERENCES

Absalom, A.R., Vereecke, H.E., and Eleveld, D.J. (2011). A hitch-hikers guide to the intravenous PK/PD galaxy. *Pediatric Anesthesia*, 21(9), 915–918.

Absalom, A. and Kenny, G.N.C. (2003). Closed loop control of propofol anaesthtesia using bispectral index: perofrmance assessment in patients receiving computer-controlled propofol and manually controlled remifentanil for minor surgery. *British Journal of Anaesthesia*, 90(6), 737–741.

Åström, K.J. and Wittenmark, B. (1984). *Computer-Controlled Systems*. Prentice Hall, Englewood Cliffs, NJ.

Caiado, D.V., Lemos, J.M., and Costa, B.A. (2012). Robust pole-placement control of neuromuscular blockade. In *Automatic Control, 2012 10th Portuguese Conference on*, 75–80.

Dumont, G.A., Martinez, A., and Ansermino, J.M. (2009). Robust control of depth of anesthesia. *International Journal of Adaptive Control and Signal Processing*, 23(5), 435–454.

Haddad, W.M., Hayakawa, T., and Bailey, J.M. (2006). Adaptive control for nonlinear compartmental dynamical systems with applications to clinical pharmacology. *Systems & Control Letters*, 55(1), 62 – 70.

Hahn, J.O., Dumont, G., and Ansermino, J. (2012). A direct dynamic dose-response model of propofol for individualized anesthesia care. *Biomedical Engineering, IEEE Transactions on*, 59(2), 571–578.

Hodrea, R., Morar, R., Nascu, I., and Vasian, H. (2013). Modeling of neuromuscular blockade in general anesthesia. In *Advanced Topics in Electrical Engineering, 2013 8th International Symposium on*, 1–4.

Mendonça, T. and Lago, P. (1998). PID control strategies for the automatic control of neuromuscular blockade. *Control Engineering Practice*, 6(10), 1225 – 1231.

Niño, J., De Keyser, R., Syafiie, S., Ionescu, C., and Struys, M. (2009). EPSAC-controlled anesthesia with online gain adaptation. *International Journal of Adaptive Control and Signal Processing*, 23(5), 455–471.

Ristic, B., Arulampalam, S., and Gordon, N. (2004). *Beyond the Kalman Filter: Particle Filters for Tracking Applications*. Artech House radar library. Artech House.

Rocha, C., Mendonça, T., and Silva, M.E. (2013). Modelling neuromuscular blockade: a stochastic approach based on clinical data. *Mathematical and Computer Modelling of Dynamical Systems*, 19(6), 540–556.

Rosen, O. and Medvedev, A. (2013). Efficient parallel implementation of state estimation algorithms on multicore platforms. *Control Systems Technology, IEEE Transactions on*, 21(1), 107 –120.

Rosen, O., Medvedev, A., and Ekman, M. (2010). Speedup and tracking accuracy evaluation of parallel particle filter algorithms implemented on a multicore architecture. In *Control Applications (CCA), 2010 IEEE International Conference on*, 440 –445.

Silva, M.M. (2011). Prediction error identification of minimally parameterized wiener models in anesthesia. In *Proc. 18th IFAC World Congress*, 5615–5620.

Silva, M.M., Mendonça, T., and Wigren, T. (2010). Online nonlinear identification of the effect of drugs in anaesthesia using a minimal parameterization and bis measurements. In *American Control Conference*, 4379–4384.

Silva, M.M., Lemos, J.M., Coito, A., Costa, B.A., Wigren, T., and Mendonça, T. (2014). Local identifiability and sensitivity analysis of neuromuscular blockade and depth of hypnosis models. *Computer Methods and Programs in Biomedicine*, 113(1), –23–36.

Silva, M.M., Wigren, T., Medvedev, A.V., and Mendonça, T. (2013). Quantification of the multiplicative uncertainty in the linearized minimally parameterized parsimonious wiener model for the neuromuscular blockade in closed-loop anesthesia. In *Control Automation, Mediterranean Conference on*, 703–708.

Silva, M., Wigren, T., and Mendonça, T. (2012). Nonlinear identification of a minimal neuromuscular blockade model in anesthesia. *Control Systems Technology, IEEE Transactions on*, 20(1), 181–188.

Söderström, T. (2002). *Discrete-time Stochastic Systems*. Springer-Verlag, London, UK.

Söderström, T. and Stoica, P. (1989). *System Identification*. Prentice-Hall, Hemel Hempstead, UK.

van Heusden, K., Ansermino, J., Soltesz, K., Khosravi, S., West, N., and Dumont, G. (2013). Quantification of the variability in response to propofol administration in children. *Biomedical Engineering, IEEE Transactions on*, 60(9), 2521–2529.

Zhusubaliyev, Z., Medvedev, A.V., and Silva, M.M. (2013). Bifurcation analysis for PID-controller tuning based on a minimal neuromuscular blockade model in closed-loop anesthesia (I). In *Decision and Control, 2013 IEEE 52nd Annual Conference on*, 115–120.